Enhancement of visible light-induced surface photo-activity of nanostructured N-TiO₂ thin films modified by Ion Implantation

Pablo Romero-Gomez,*[1-2] Carmen Lopez-Santos,[1] Ana Borras,[1] Juan Pedro Espinos,[1] Alberto Palmero,[1] Agustin R. Gonzalez-Elipe[1]

1- Instituto de Ciencia de Materiales de Sevilla (CSIC, U. Sevilla), C/ Américo Vespucio 49, E-41092 Sevilla, Spain.
2- ICFO-The Institute of Photonic Sciences, Mediterranean Technology Park, 08860 Castelldefels, Barcelona, Spain.

ABSTRACT

This work reports the morphological and chemical modifications induced in TiO_2 thin films by bombardment with high energy N^+ ions at different temperatures and their different photo-activity responses after implantation under visible and UV light illumination. When implanted samples are illuminated with visible light, no dye photo-decolouration takes place despite that light transformed the surfaces from hydrophobic to hydrophilic. In agreement with the Wenzel model of wetting, correlation is found between visible light photo-activity and film morphology. We conclude that the photo-activity response can be separated into shallow and Schottky barrier photo-activity, this latter involving a thicker layer of material.

Keywords

N-TiO_2, light induced wetting, ion implantation, surface photo-activity, PECVD, Wenzel model.

*Electronic mail: pablo.romero@icfo.es, tel. +34 954 48 95 28, Instituto de Ciencia de Materiales de Sevilla (CSIC, U. Sevilla), C/ Américo Vespucio 49, E-41092 Sevilla, Spain.

TiO$_2$ is a well-known material because of its wide use in numerous applications such as photo-anode in photo-electrochemical cells, photo-catalyst, anode in hybrid photovoltaic cells or coating for self-cleaning applications [1-4]. Yet, TiO$_2$ has an important drawback regarding solar energy applications as it only shows a selective response to the UV region of the solar spectrum, which only accounts for 5% of the collected light on earth. To address this problem, many works have attempted to dope this wide band gap semiconductor (3.2 eV) [5] to shift its photo-response onset towards the visible light region [6-11]. According to Asahi et al. [6], the presence of a small amount of N in the TiO$_2$ network alters the band gap structure and triggers the photo-response of the material under visible light illumination. After this seminal work, many other papers have dealt with this issue [12-21] finding that, besides composition and crystallographic structure [22], surface morphology could also play an important role in the photo-activity of this oxide. However, experimental evidences on this issue are still under discussion as their relevance seems to strongly depend upon the particular photo-activity test employed [23].

A typical surface photo-activity test concerns the wetting behaviour of TiO$_2$ surfaces upon illumination: as it was first demonstrated by Wang et al. [3], the wetting behaviour of flat TiO$_2$ surfaces evolves from a hydrophobic to a superhydrophilic state when samples are illuminated with UV-light. Although this study was carried out more than a decade ago, the physicochemical processes responsible for the reversible conversion between these two states are still a matter of debate [24-31]. For instance, in previous works on nanostructured surfaces, we have shown that surface roughness or the nitrogen doping state are critical factors affecting both, the WCA of the original samples before illumination [32] and their response when using visible light [33,34]. A first goal of the present work is to study the effect of visible light illumination of N-doped TiO$_2$ in an attempt to unravel the effect of both, surface topography and chemistry, on the wetting behaviour. For this purpose, we have considered the classical model of Wenzel to account for the influence of surface roughness on the wetting contact angle. In the course of this investigation, we have found that the light-induced hydrophobic/superhydrophilic conversion is exclusively linked to the chemical and morphological properties of the outmost surface layers, which tentatively we will called *shallow photo-activity*, while other photo-activity tests, such as the photo-catalytic degradation of dye molecules, involve a relatively thicker layer of surface material with well-defined TiO$_2$ stoichiometry. Consequently, we conclude that each photo-active response of the material is mediated through different mechanisms acting on different spatial scales on the outmost surface layers of the films.

Nanostructured N-TiO$_2$ surfaces were prepared in two steps: first, TiO$_2$ thin films were deposited by plasma enhanced chemical vapour deposition (PECVD) at 523 K. Details about the morphology, microstructure and other characteristics of these thin films, as well as the description of the deposition

2

technique, have been reported previously [34]. Films displayed an anatase structure with a high degree of crystallinity and showed a clear columnar microstructure perpendicular to the substrate. In a second step, films were exposed to high energy nitrogen ions by means of a particle accelerator. These ion implantation experiments were carried out with the high current ion implanter DANFYS 1090-200(DANFYSIK A/S, Jyllinge Denmark) at the Institute of Ion Beam Physics and Materials Research in the Forschungszentrum Rossendorf, Germany, being the maximum acceleration voltage of this machine 200 kV. For equal ion doses and impingement angle, implantations were carried out at two different substrate temperatures. The experimental conditions utilized in each case are summarized in Table I: Sample A is a test sample analysed just after deposition. Sample B represents a film deposited under the same conditions as sample A, experiencing the N^+ ion implantation (keeping the film at room temperature during the procedure) afterwards. The ion range within the material in these conditions has been estimated using the well-known software SRIM [35], yielding a value of ~100 nm. Following the well-known effects of implanted ions in TiO_2 [36], we assume that a layer with similar thickness has been subjected to a considerable lattice damage resulting in the formation of a high concentration of oxygen vacancies, point defects in the network and other related effects. Furthermore, as an additional amorphization of the film may appear along the ion tracks [37,38], we also analysed sample C, where the ion implantation conditions were the same as those employed for sample B, but keeping the film temperature at 400 ºC throughout the whole procedure this time, just to ensure that the film could recrystallize into the anatase structure.

Rutherford Backscattering Spectroscopy (RBS) has been utilized to assess the atom distribution profile in the films and in their implanted zones. Experiments were carried out in a 3 MeV tandem accelerator at the CNA (Sevilla, Spain) with a beam of 1.5−2.0 MeV alpha particles, accumulated doses about 1.5 μC, and ∼1 mm beam spot diameter. The RBS spectra were simulated with the SIMRNA software [39]. Results indicate that nitrogen ion bombardment caused the oxygen depletion in the implanted layer: Figure 1 shows the experimental and simulated spectra of samples A, B and C. A comparative assessment of the shape of the Ti signal in Figure 1 clearly shows that the implanted layer in Sample B (around 100 nm) is oxygen depleted as indicated by the relative increase in the intensity of the Ti signal closer to the surface. A similar effect is observed in sample C where the variation in the intensity of the Ti signal is smoother. In other words, it seems that the implanted zones in samples B and C present some oxygen depletion resulting from an extensive formation of oxygen vacancies. This result agrees with surface conductivity measurements carried out by the four-point probe test. For these measurements a Keithley 617 Electrometer and a Hewlett-Packard 34401 A voltammeter were used to apply a voltage ranging between -0.25 and 0.25 V to two external probes and to measure the current flowing between two internal probes. In this way, the surface resistivity of the three samples (see Table 1) shows a completely different behaviour: sample A has a highly

resistive character, whereas samples B and C show very low resistivity, which again agrees with the observed oxygen depletion of the network lattices.

The surface state of samples after nitrogen implantation was assessed by X-ray Photoelectron Spectroscopy (XPS) recorded on a VG ESCALAB 210 spectrometer working under pass energy constant conditions. The Mg Kα line was used for excitation of the spectra, calibrated in binding energy (BE) by referencing to the C1s peak due to contamination taken at 284.6 eV. In all the samples, the O(1s) and Ti(2p) spectra were typical of TiO_2 thin films [40], a feature that indicates that the outmost surface layers within the thickness analysed by the XPS technique have become fully oxidized due to the exposure and handling of the films in the atmosphere. Interestingly, the XPS measurements also show the existence of nitrogen species on the surface of the B and C films. Figure 2 shows the deconvolution of the N1s photoemission spectra recorded for the three samples: sample A does not contain nitrogen, a fact that is expected as it did not undergo the N^+ ion implantation. Samples B and C display similar spectral shapes, indicating that, unlike sample A they possess N on the outmost surface layers with similar chemical state. A rough fitting analysis of these two spectra is possible by assuming three components centred at 396.2, 398.8 and 401.2eV with area ratios of 1:0.24:0.14 and 1:0.45:0.19 for samples B and C, respectively. Despite some controversy in the literature concerning the assignment of these three components [40] a rather accepted consensus is that the wide band around 396.2 eV is associated with diamagnetic N(III) species substituting O(II) sites. Meanwhile, the N1s peaks at around 398.8 and 401.2 eV have been assigned to interstitial N species [41-43], possibly bound to lattice oxygen in a kind of NO-like units. The difference between these two latter states seems to be the type of interstitial centre occupied by the nitrogen in the TiO_2 structure [37].

The surface morphology of the films was highly affected by the ion implantation: Figure 3 shows the atomic force microscopy (AFM) images of the three investigated samples. These images were collected in an AFM dimension 3100 from Digital Instrument in tapping mode using high frequency levers, and processed with the WSxM free available software from Nanotec [48]. Roughness of the films, expressed as the root mean square (RMS) value of the surface heights, has been calculated from the images by using this software. This analysis concluded that sample A possesses a granular structure with a RMS of 1.9 nm [34], whereas sample B (where the ion implantation took place at room temperature) shows an almost flat surface topography with an estimated value of the RMS around 0.2 nm. This is consistent with the field emission scanning electron microscopy (FESEM) characterization of these samples, which indicates that they present a sponge-like microstructure underneath, capped by a quite flat surface [38]. Meanwhile, sample C, with a RMS value of 4.7 nm, is characterized by a tilted nanorod microstructure that has been attributed to the N^+ implantation at 400 ^0C, and whose origin was explained elsewhere [38].

4

By taking into account the previous analysis, a reasonable schematic representation of the composition profiles of samples A, B and C is presented as insets in Figure 1: sample A is fully stoichiometric, while samples B and C present three different zones: i) few surface layers with a TiO_2 stoichiometry and some nitrogen species, followed by ii) a zone depleted in oxygen where, in agreement with previous studies [38], nitrogen is mostly in the chemical form of nitride species, and iii) a third zone that corresponds to the region of the film not affected by the N^+ ions, and whose composition is again stoichiometric TiO_2. According to this layer distribution, samples B and C possess very different surface roughness but very similar morphological and chemical structures: the two films share a similar surface composition (N-doped TiO_2) and present a second layer underneath depleted in oxygen that extends along the depth where a Schottky Barrier is typically formed.

The photo-activity of samples A-C was first evaluated by tracking the change in the WCA upon visible and UV light irradiation. The recovery of the WCA in darkness after illumination complemented these tests. In parallel, the photo-catalytic activity of these samples was tested by following their capability to decolorize a solution with a dye [23,33]. In the first place, measurements of water contact angle (WCA) of samples A, B and C were carried out by the Young method by dosing small droplets of deionized and bidistilled water on the surface of the samples illuminated for increasing periods of time. During the experiments, a metal foil acting as a shutter was used to close and open the lamp output. The reported results correspond to samples that were stored in dark in a desiccator, at least for two months, before testing their photo-activity. Illumination of the samples was carried out with a Xe discharge lamp with photon intensity at the position of the samples of 2 W cm^{-2} for the complete spectrum. An infrared filter (i.e. a water bath) was kept between the lamp and the samples to prevent any possible heating by the infrared radiation. On the other hand, dye degradation experiments under visible and UV illumination were carried out in a home-made experimental set-up consisting of a small cell made of quartz (total volume 3 cm^3) where 2 cm^3 of a 3.5×10^{-5} M solution of methyl orange dye was placed together with a piece of a silicon substrate (1×0.8 cm^2) with the thin film deposited on its surface. The intensity of the UV + visible radiation at the position of the cell was 1.8 W (i.e., approximately 0.3 W cm^{-2} for photons with $\lambda < 380$ nm). Visible illumination was carried out by placing a filter (i.e., $\lambda > 380$ nm) between the Xe discharge lamp and the reaction vessel. The intensity of the visible radiation at the cell position was 160 mW cm^{-2}. Additional details about this experiment can be found in a previous publication [23].

The dye degradation experiments showed that sample A was able to decolorize the dye solution upon irradiation with a full range lamp (i.e. emitting in the UV and visible range) [23], while samples B and C did not induce any photo-catalytic degradation under similar conditions (result not shown). By contrast, the illumination of the samples with either UV or visible light rendered a clear change in their WCA. Figure 4 shows the time evolution of the WCA of these samples that were first irradiated

with visible light (zone 1), then with UV light (zone 2) and finally left in the dark (zone 3). The three samples present initially a WCA higher than 90º, thus depicting a hydrophobic behavior. Furthermore, we link the high initial WCA of sample C (130^0) to the high roughness of the film (4.7 nm) in agreement with the premises of the Wenzel model of surface wetting [44]. Most remarkable in Figure 4 is that samples B and C experienced a continuous decrease in WCA when they were irradiated with visible light, a feature that must be linked with the incorporation of nitrogen within a stoichiometric TiO_2 lattice at the outmost surface layers of material. It is worth noting that after contacting the surface of samples A, B or C with water, the XPS spectra taken after drying did not show any significant difference with respect to the original samples, except for a broadening in the shape of the O1s spectra in the high BE side that we attribute to some additional hydroxylation of the surface.

In line with previous results [11, 23, 33, 46], the described experiments confirm that WCA light induced-changes and photo-catalytic activity are not necessarily equivalent for testing the photo-activity of TiO_2. According to the schemes in Figure 1, the outmost surface layers of all samples (i.e. within the penetration range of the XPS technique) present a TiO_2 stoichiometry, with samples B and C containing a certain concentration of N-O-like species. The WCAs of the three samples respond to the illumination of light, UV (sample A) and UV and visible (samples B and C). Yet, only sample A, with a TiO_2 stochiometry throughout the whole sample thickness, presents photo-catalytic activity towards the degradation of dye molecules. According to previous investigations in our laboratory, these results confirm that there is a TiO_2 photo-activated surface mechanism responsible for changing the surface wettability behavior, even when the film do not show any noticeable response when performing dye decoloration tests [23]. In this regard, the absence of photo-catalytic activity in samples B and C must be related with the fact that their inner layers are sub-stoichiometric and, therefore, present a high concentration of oxygen vacancies. Under these conditions, it seems that the electron-hole photo-excitation processes are not efficient and that most carriers must recombine at the lattice defects, so they do not reach the surface. We tentatively called *Schottky Barrier Driven Photo-activity* the type of photo-catalytic activity that requires the migration of photo-generated electron-hole pairs from the interior of the material up to the surface as. Therefore, our results here confirm that photo-induced WCA variations only involve mechanisms at the very first outmost monolayers of the material [33], a response that we tentatively call *shallow photo-activity*.

Our results also reveal that a shallow photo-active response affecting the WCA can be induced by illuminating N-doped TiO_2 with visible light, with WCA steady-state values around 50° and 20° for samples B and C, respectively, whereas superhydrofilicity is attained with UV light. The recovery in the dark of the WCA of the three samples confirms the full reversibility of this transformation. Recently, the visible photo-activity of N-doped TiO_2 has been related with the presence of the N1s

6

species at around 400 eV of binding energy (in our case the N1s peaks at around 398.8 and 401.2 eV), attributed to N-O like species [33,45-47]. Our WCA photo-activity results confirm this previous attribution and sustain that these species can be involved in the visible light surface activation of TiO_2. Furthermore, since samples B and C present similar concentration of nitrogen, the different final state of WCA after visible light irradiation must be attributed to their different roughness: according to the Wenzel model, the WCA of either hydrophobic or hydrophilic samples experience an additional increase (hydrophobicity) or decrease (hydrophilicity) with respect to the WCA of a flat surface of equivalent composition. Therefore, the tendency in the WCA of the original samples before irradiation (i.e., WCA (Sample A) < WCA (Sample B) < WCA (Sample C)) and for samples B and C after visible irradiation (WCA (Sample B)>WCA (Sample C)) must be linked with the progressive increase in surface roughness from sample A to C.

In summary, the experiments above confirm that N-doped TiO_2 presents surface photo-activity when illuminated with visible light even if it is photo-catalytically inert under both visible or UV light illumination. Moreover, our results have also shown that the changes in the WCA can be tuned by modifying the surface roughness. The implications of these two features for microfluidic applications or for the fabrication of self-cleaning surfaces in interiors (i.e., in the absence of UV light) are obvious and should permit the fabrication of smart responsive surfaces with a controllable surface wetting. Overall, we demonstrate that shallow and Schottky barrier driven photo-activities are not equivalent and that, consequently, they must be studied separately.

REFERENCES:

1   Hurum, D.C.; Agrios, A. G.; Gray, K. A., J. Phys. Chem. B 2003, 107, 4545-4549.

2   Huang, W.X.; Deng, W.; Lei, M.; Huang, H., Appli. Surf. Sci. 2011, 257, 4774-4780.

3   Wang, R.; Hashimoto, K.; Fujishima, A.; Chikuni, M.; Kojima, E.; Kitamura, A.; Shimohigoshi, M.; Watanabe, T., Nature 1997, 388, 431-432.

4   Betancur R.,Martınez-Otero A., Elias X., Romero-Gomez P., Colodrero S., Miguez H.,Martorell J., Sol. Energy Mater. Sol. Cells 2012, 104, 87–91.

5   Chen, X.; Mao, S.S., Chem. Rev. 2007, 107, 2891-2959.

6   Asahi, R.; Morikawa, T.; Ohwaki, T.; Aoki, K.; Taga Y., Science 2001, 293, 269-271.

7   Sakthivel, S.; Janczarek, M.; Kirsch, H. J., Phys. Chem. B 2004, 108, 19384.

8   Diwald, O.; Thompson, T. L.; Zubkov, T.; Goralski, E. G.; Walck, S. D.; Yates, J. T., J. Phys. Chem. B 2004, 108, 6004.

9   Nosaka, Y.; Matsushita, M.; Nasino, J.; Nosaka, A. Y., Sci. Technol. AdV. Mater. 2005, 6, 143-148.

10   Gracia F.; HolgadoJ. P.;CaballeroA.;Gonzalez-ElipeA. R., J. Phys. Chem. B, 2004, 108, 17466–17476.

11   Romero-Gomez P.; Hamad S.;Gonzalez J. C.;Barranco A.;   J. P.;Cotrino J.; Gonzalez-Elipe A. R., J. Phys. Chem. C, 2010, 114, 22546–22557

12   Di Valentin, C.; Pacchioni, G.; Selloni, A.; Livraghi, S.; Giamello, E., J. Phys. Chem. B 2005, 109, 11414-11419.

13   Diwald, O.; Thompson, T. L.; Goralski, E. G.; Walck, S. D.; Yates, J. T., J. Phys. Chem. B 2004, 108, 52-57.

14   Yates, H. M.; Nolan, M. G.; Sheel, D. W.; Pemble, M. E., J. Photochem. Photobiol. A: Chem. 2006, 179, 2013-223.

15   Livraghi, S.; Paganini, M. C.; Giamello, E.; Selloni, A.; Di Valentin, C.; Pacchioni, G., J. Am. Chem. Soc. 2006, 128, 15666-15671.

16   Lu, JW.; Su, Fl.; Huang, Zq.; Zhang, CX. ; Liu, Y.; Ma, XB.; Gong, JL., RSC Adv. 2013, 3, 3, 720-724.

17   Barolo, G. ; Livraghi, S.; Chiesa, M.; Paganini, MC.; Giamello, E., J. Phys. Chem. C. 2012, 116, 20887-20894.

8

18   Pelaez, M.; Nolan, NT.; Pillai, SC.; Seery, MK.; Falaras, P.; Kontos, AG.; Dunlop, PSM.;
      Hamilton, JWJ.; Byrne, JA.; O'Shea, K.; Entezari, MH.; Dionysiou, DD., Appl. Cat. B-Env.
      2012, 125, 331-349.

19   Selvam, K.; Balachandran, S.; Velmurugan, R.; Swaminathan, M., Appl. Cat A Gen. 2012,
      413,213-222.

20   Huang, D.; Miyamoto, Y.; Ding, J.; Gu, J.; Zhu, S.; Liu, Q.; Fan, T.; Guo, Q.; Zhang, D., Mat.
      Lett. 2011, 65, 326-328.

21 Livraghi, S.; Paganini, M. C.; Giamello, E.; Selloni, A.; Di Valentin,C.; Pacchioni, G., J. Am.
      Chem. Soc. 2006, 128, 15666-15671

22   Huang, T.; Huang, W.; Zhou, C.; Situ, Y.; Huang, H., surf. coat. technol 2012, 213, 126-132.

23   Rico, V.; Romero, P.; Hueso, J.L.; Espinos, J.P.; Gonzalez-Elipe, A.R., Catal. Today, 2009,
      143, 347-354.

24   Zubkov, T.; Stahl, D.; Thompson, T. L.; Panayotov, D.; Diwald, O.; Yates, J. T., J. Phys.
      Chem. B 2005, 109, 15454-15462.

25   Thompson, T. L.; Yates, J. T., Chem. Rev. 2006, 106, 4428.

26   Nakajima, A.; Koizumi, S.; Watanabe, T.; Hashimoto, K., Langmuir 2000, 16, 7048-7050.

27   Sun, W.; Zhou, S.; Chen P.; Peng, L., Chem. Commun. 2008, 5, 603–605

28   Sahoo, M.; Mathews, T.;   Antony, R.P.; Krishna, D. N.;   Dash, S.; Tyagi, A. K., *Mater.
      Interfaces*, 2013, 5, 3967–3974.

29   Borras, A.; Barranco, A.; Gonzalez-Elipe, A.R., Langmuir, 2008, 24, 8021–8026.

30   Fujishima, A; Zhang, XT., Comptes Rendus Chimie, 2006, 9, 750-760.

31   Rengifo-Herrera, Julian A.; Pierzchała K.;Sienkiewicz A.;   L.;Kiwi J.; MoserJacques E.;
      Pulgarin C., J. Phys. Chem. C, 2010, 114, 2717–2723.

32   Borras,A.; Gonzalez-Elipe, A.R., *Langmuir* 2010, 26,15875–15882.

33   Romero- Gomez, P.; Rico, V.; Borras, A.; Barranco, A. ;Espinos, J. P.; Cotrino, J.;Gonzalez-Elipe, A. R., *J. Phys. Chem. C* 2009, 113, 13341–13351.

34   Borras, A.; Lopez, C.; Rico, V.; Gracia, F.; Gonzalez-Elipe, A.R., J. Phys. Chem. C 2007, 111, 1801-1808.

35   http://www.srim.org/.

36   Diwald, O.; Thompson , T. L.; Goralski, E. G.; Walck, S. D.; Yates, Jr. J. T., J. Phys. Chem. B 2004, 108, 52-57.

37   Romero-Gomez, P.; Palmero, A.; Yubero, F.; Vinnichenko, M.; Kolitsch, A.; Gonzalez-Elipe, A.R., Scr. Mater. 2009 60, 574–577.

38   Romero-Gomez, P.; Palmero, A.; Ben, T.; Lozano, J. G.; Molina, S. I.; González-Elipe, A. R., Phys. Rev. B. 2010, 82, 115420.

39   Mayer M. *Technical Report 9* Max-Planck-Institut für Plasmaphysik 1997, 113

40   Romero-Gomez, P. ; Rico, V.; Espinos, J.P.; Gonzalez-Elipe, A.R.; Palgrave, R.G.; Egdell, R.G., Thin Solid Films 2011, 519, 3587-3595.

41   Mi, L.; Xu, P.; Wang, P.N., Appl. Surf. Sci. 2008,255, 2574-2580.

42   Graciani, J.; Alvarez, L.J.; Rodriguez, J.A.; Sanz, J.F., J. Phys. Chem. C 2008, 112, 2624-2631.

43   Che, M.; Naccache, C., Chem. Phys. Lett. 1971, 8, 45-48.

44   Wenzel, R.N., J. Phys. Coll. Chem. 1949, 53, 1466-1467.

45   Napoli, F.; Chiesa, M.; Livraghi, S.; Giamello, E.; Agnoli, S.; Granozzi, G.; Pacchioni, G.; Di Valentin, C., Chem. Phys. Let., 2009, 477, 135-138.

46   Di Valentin, C.; Pacchioni, G.; Selloni, A., Phys Rev. B, 2004. 70, 8.

47   Hu Y., Liu H., Rao Q., Kong X., Sun W., Guo X., J. Nanosci Nanotechnol. 2011, 11, 3434-3444.

48   Horcas I., Fernández R., Gomez-Rodríguez J.M., Colchero J., Gomez-Herrero J., Baro A.M., Rev. Sci. Instrum. 2007, 78, 013705.

49   Romero-Gomez, P.; Borras, A.; Barranco, A.; Espinos, J. P.; Gonzalez-Elipe A. R. ChemPhysChem 2011, 12, 191 – 196

Table Caption

	Energy (KeV)	Incident angle (^{0})	Dose Ions/cm^{-2}	Temperature (^{0}C)	RMS (nm)	WCA (visible, º)	Resistivity (Ω·cm)
A			Not irradiated		1.9	100	insulator
B	60	45	$2.4 \cdot 10^{17}$	RT	0.2	52	3.1
C	60	45	$2.4 \cdot 10^{17}$	400	4.7	22	0.3

Table I. Summary of the N$^+$ implantation conditions (energy, incident angle and dose of the ions along with the film temperature) and measured properties of the samples (roughness, water contact angle and four points probe resistivity under visible light illumination).

Figure captions

Figure 1. Experimental and simulated RBS spectra of samples A, B and C. The insets depict schematic representations of the in-depth evolution of stoichiometry for the three investigated samples, as deduced from the RBS and XPS results.

Figure 2. N1s photoelectron spectra obtained for samples A, B and C (Black lines). Elemental bands employed in the fitting are plotted in grey

Figure 3. AFM images of a) sample A, b) sample B and c) sample C. The arrow in Figure 3c indicates the direction of the impinging ions during implantation. The scale of the color bar is in nanometers.

Figure 4.Time dependence of the WCAs of a) sample A, b) sample B and c) sample C, illuminated with visible and UV light and subsequently left in the dark. Lines are plotted to guide the eyes. The circles show the wetting contact angle values measured onto samples illuminated with visible light. Images of the water droplets are inserted in the plots.
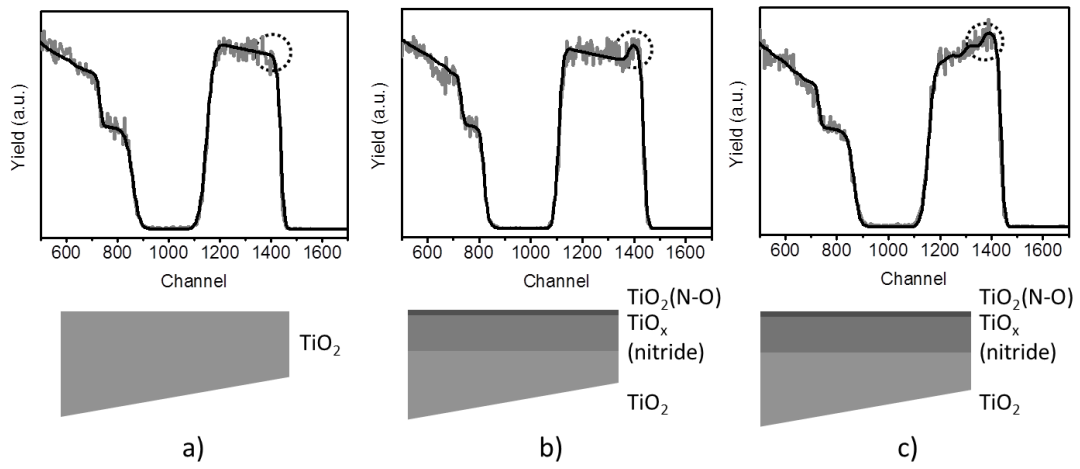
Figure 1

Figure 2

Figure 3

Figure 4